Optimal Collector System Planning for Offshore Wind Farm Based on Bidirectional Flow Conservation Method

Shuaifeng Wang, Sheng Huang, *Member*, *IEEE*, Juan Wei, *Member*, *IEEE*, Qiuwei Wu, *Senior Member*, *IEEE*, Wenbo Tang, Lu Zhou, and Shoudao Huang

***Abstract*—High-reliability double-sided ring collector systems have been widely implemented in offshore wind farms (OWFs). It is challenging to achieve a globally optimal network topology and a cable capacity rating for the OWF collector system (CS) simultaneously. This paper proposes an optimal collector system planning (CSP) method for OWF with double-sided ring topology based on bidirectional flow conservation method to minimize cable costs and total power losses. By analyzing the power flow direction after faults, all fault scenarios are summarized into two fault conditions. The bidirectional flow conservation method is developed to reveal the matching mechanism between different cable sequence positions and their optimal ratings, considering the minimal rating requirements. The complex high-dimensional CSP problem, which involves the coupling characteristics of different cable parameters and system power flows, is convexified by equivalent alternative methods into a mixed-integer quadratic programming (MIQP) to guarantee a global optimal solution within feasible computation time, improving the solvability and practicality. The effectiveness of the proposed optimal CSP method has been validated in MATLAB.**

***Index Terms*—Collector system planning (CSP), offshore wind farm, cable capacity rating, network topology, mixed-integer quadratic programming (MIQP), power flow.**

I. Introduction

WIND energy has emerged as a mainstream clean energy source, driven by its low life-cycle emissions and economic competitiveness [1], [2]. Offshore wind farms (OWFs) have attracted considerable global attention compared with onshore wind farms due to superior wind conditions and more favorable locations for capturing wind energy resources [3]. The global installed capacity of offshore wind power has reached 8.8 GW, marking a 16% year-on-year increase [4]. However, the high investment, operation, and maintenance costs associated with OWFs pose significant challenges for the offshore wind power industry.

The costs associated with collector and transmission systems typically constitute 20% of the total investment cost in OWFs [5]. Collector system planning (CSP) is particularly variable, involving decisions on network topology, selection of cable type, etc. [6]. CSP also influences the power loss and operation costs. Therefore, numerous studies have focused on designing an optimal collector system (CS) for OWFs.

Radial topology is a favored choice for offshore wind farm collector systems (OWF-CSs) owing to its simplicity and low investment costs [7], [8]. In [9], a graph-theoretic minimum spanning tree algorithm is used to compute the minimum total trenching length of the CS. In [10], a bi-level optimization framework is proposed to jointly optimize the wind turbine (WT) micro-siting and cabling based on the non-dominated sorting genetic algorithm-III and binary particle swarm optimization algorithm. To obtain the global optimal cabling topology, the Benders decomposition algorithm is used for the CSP [5], [11]. Large-scale OWFs include more than 100 WTs, which make the CSP problem more difficult to solve. The mathematical program solver (IBM ILOG CPLEX Optimization Studio [12]) is used to solve the large and difficult mixed-integer quadratic programming (MIQP) problem [13], [14]. However, the radial topology fails to ensure the uninterrupted operation of downstream WTs in the event of a cable failure within an OWF [15]. Due to the transmission distance between offshore and onshore substations, which often exceeds 80 km [16], the mean time to restoration is extended, resulting in increased power losses.

High-reliability double-sided ring CSs have been commercialized and widely implemented for long-distance and large-scale OWFs (e. g., London Array OWF). The sweep and Clarke-Wright saving algorithm is introduced to optimize the cable topology and minimize investment cost [17]. In [18], the single parent genetic algorithm and multiple traveling salesman solution technique are integrated and applied. A

Manuscript received: December 10, 2024; revised: March 26, 2025; accepted: May 20, 2025. Date of CrossCheck: May 20, 2025. Date of online publication: June 11, 2025.

This work was supported by the National Key R&D Program of China (No. 2022YFF0608700), the National Natural Science Foundation of China (No. 52207050), and Basic Research Funds for Central Universities (No. 531118010949).

S. Wang, S. Huang (corresponding author), J. Wei, W. Tang, and S. Huang are with the College of Electrical and Information Engineering, Hunan University, Changsha 410082, China (e-mail: sf_wang@hnu.edu.cn; huangsheng319@hnu.edu.cn; weijuanba@hnu.edu.cn; 147206621@qq.com; hsd1962@hnu.edu.cn).

Q. Wu is with Tsinghua-Berkeley Shenzhen Institute, Tsinghua Shenzhen International Graduate School, Tsinghua University, Shenzhen 518055, China (e-mail: quiwudtu@gmail.com).

L. Zhou is with Huadian Electric Power Research Institute Co., Ltd., Hangzhou 310030, China (e-mail: lu-zhou@chder.com).

DOI: 10.35833/MPCE.2024.001323

multi-substation incorporation structure is designed to reduce transformer capacity within each substation to enhance economic and reliability benefits for OWFs with multiple substations [19]. Moreover, a two-layer hybrid CSP is proposed to improve economic efficiency and stabilized outputs of an OWF with 160 Vestas 112 3.0 MW WTs [20]. The optimization effects by the heuristic algorithms depend on the initial network and algorithmic framework, and the global optimal solution cannot be obtained. A global optimal algorithm based on an MIQP model is proposed to minimize cabling costs and power losses to address this issue [21]. However, only one type of cable is considered. The unified rating matching leads to excessive flow redundancy and higher investment costs.

When planning OWF-CS with a double-sided ring topology, it is common practice to quantify the operation costs over the entire service life in terms of network losses. In the realm of related research, the DisFlow model has been utilized, which calculates losses based on the mixed-integer second-order cone programming (MISCOP) and is employed to design the optimal CSs with a radial topology structure [22]. The DC power model is used to calculate power losses within single-cable wind farm collection systems [23]. Furthermore, for single-substation wind farms, a pre-processing strategy is integrated into the integer linear programming (ILP) to handle the multi-cable applications [24]. However, network losses do not directly influence the CSP result.

The cable optimal rating (COR) can be defined as the minimum capacity that can support all its downstream WTs in the event of a single-cable fault, which means that the cable needs to meet the COR requirements [18]. Figure 1 illustrates the double-sided ring topology of OWF-CS with two different rating requirements of cable: one with a unified rating requirement of cable and the other with a COR requirement. For the unified rating requirement, all the cables need to support all the WTs in the loop. The rating requirements of all cables are the same. The COR of each cable is symmetrical in a ring topology and increases as the cable is closer to the substation [20]. For instance, in Fig. 1(b), if cable Br1 fails, the collection route for wind power is Br2-Br3-Br4-Br5-Br6-Br7-Br8-S, where S denotes the substation. Cable Br8 must support 7 WTs, while Br7 needs to support 6 WTs. Therefore, the COR design can reduce redundancy and improve economic efficiency.

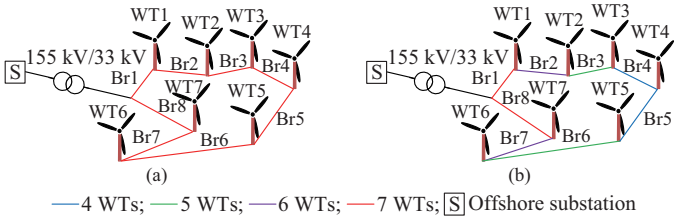

Fig. 1. Double-sided ring topology of OWF-CS. (a) Unified rating requirement. (b) COR requirement.

The CSP for double-sided ring topology is typically formulated as a two-dimensional NP-hard capacitated vehicle routing problem (CVRP). When the COR is considered, three new challenges arise. ① The cable variable will become a three-dimensional (3D) variable incorporating the start point, end point, and cable type. ② The resistor and conductance of each cable cannot be predetermined, resulting in power loss being a high-degree function. ③ Cables in the same location can be of different types depending on the entire OWF-CS topology. The cable type influences investment cost, which in turn affects the OWF-CS topology. This coupled relationship between cable type and OWF-CS topology further complicates the CSP problem. Therefore, optimal CSP is a high-dimensional, high-degree, and strongly coupled problem, currently lacking a suitable global optimal solution. The heuristic cable rating matching method [18]-[20], which avoids complex mathematical modeling, appears to be the first choice and even the only viable choice for the optimal CSP with double-sided ring topology.

To address the above issues, this paper proposes an optimal CSP method for OWFs with double-sided ring topology based on bidirectional flow conservation method. The main contributions of this paper are as follows.

1) An optimal CSP method based on bidirectional flow conservation method is proposed to minimize the cable costs and total power losses over the service life for OWF-CS with the double-sided ring topology. Compared with the traditional CSP, the proposed optimal CSP can ensure the theoretically global optimality of the solution and avoid excessive flow redundancy, thereby improving the economic efficiency of the OWF.

2) All fault scenarios are first summarized into two fault conditions by analyzing the power flow direction after a fault. The bidirectional flow conservation method is developed to establish the matching rules between the different cable sequencing positions and CORs, which can plan the OWF-CS topology while satisfying the COR requirements. Regardless of the change of OWF-CS topology, the cable type can be determined on its sequencing position.

3) The equivalent alternative methods are implemented to achieve cable sequencing position and power loss convexification. The complex high-dimensional non-linear problem involves the coupling characteristics between different cable parameters and system power flows, which can be formulated as the MIQP for achieving an exact optimal solution within a feasible computation time, while enhancing solvability and practicality.

The remainder of this paper is organized as follows. Section II presents the framework of CSP. Section III outlines the bidirectional flow conservation method. Section IV describes the CSP formulation. Section V describes the model convexification and solution. Section VI discusses case studies, followed by the conclusion in Section VII.

II. Framework of CSP

For a practical OWF, the elements including the offshore substation, WTs, and cables can be analogous to the depot, customer points, and routes of the capacitated vehicle routing model [25]. The three-stage planning framework of the OWF-CS is illustrated in Fig. 2, including the pre-deterministic stage, computational stage, and verification stage. The planning method can avoid excessive flow redundancy and enhance the economic efficiency of the OWF.

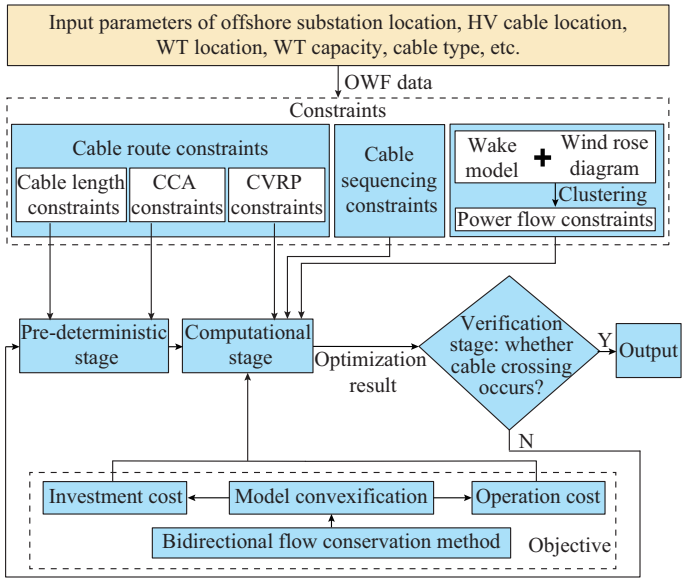

Fig. 2. Three-stage planning framework of OWF-CS.

In the pre-deterministic stage, to facilitate maintenance and prevent failure expansion [26], the cable length constraints and cable crossing-avoidance (CCA) constraints between medium-voltage (MV) and high-voltage (HV) cables can be predefined. Cables that violate these constraints are considered non-candidate cables and are addressed to reduce topological connection variables, which will be detailed in Section IV-C.

In the computational stage, the CVRP, cable sequencing, and power flow constraints, and the investment and operation cost functions are formulated into the MIQP model. The bidirectional flow conservation method is developed to realize matching between cables and their COR, and obtain the most economical solution. The investment and operation cost functions are convexified using equivalence alternative methods. The output power of each WT is calculated based on the wake model and wind rose diagram to determine the power flow of the OWF-CS.

The number of CCA constraints associated with MV-MV cables is significant, so these constraints are treated as evaluation criteria in the verification stage to avoid extended modelling time. If cable crossings occur in the optimization result, the corresponding CCA constraints are added to recalculate the CSP problem.

III. Bidirectional Flow Conservation Method

The model of flow conservation [27] is widely studied and applied in the topology reconfiguration of radial distribution networks [28] and the topology planning of radial wind farm CS [29]. The flow conservation model not only ensures the radial structure of the network, but also calculates the flow of each cable. Unlike the fixed unidirectional power flow in radial networks, which flows from the feeder end towards the substation, the power flow direction in ring topology changes based on the location of the fault point. Therefore, a new model is needed for ring topology to ensure that each cable can support all its downstream WTs in the event of any single-cable fault.

A. The Maximum Sequencing Position of Cable

In a ring topology, when a cable fails, the circuit breakers at both ends of the cable operate to isolate the fault [23]. The network operates in a radial topology structure after fault isolation. The sequencing position of a cable is defined as the number of downstream WTs that it must support. For example, if cable Br8 fails, Br1 has 7 downstream WTs, and Br2 has 6. On the other hand, if cable Br7 fails, Br2 has 5 downstream WTs, and Br8 has 1. The maximum sequencing position of a cable is the highest sequencing position that the cable attains in all fault scenarios. By making sure that the rating of each cable is equal to its maximum sequencing position, it can be ensured that each cable can support all its downstream WTs in the case of any single-cable fault.

Analysis through all examples shows that only when the cables connected to the substation fail may the cables have the maximum sequencing position. Therefore, it is only necessary to discuss two fault conditions. Assuming the cable Br1 fails, the sequencing position of cable Br1 is 0; while for cable Br8, it is 7. Conversely, if the cable Br8 fails, the sequencing position of cable Br1 is 7; while for cable Br7, it is 0. This maximum sequencing position of cables Br1 and Br2 is 7. The maximum sequencing position of each cable can directly correspond to its COR requirement.

B. Illustration of Bidirectional Flow Conservation Method

As illustrated in Fig. 3, assuming that the positive direction of virtual power flow is clockwise and the output power of a WT is 1, (1) and (2) indicate that the power flowing out of it is one more than that flowing into it for each WT i in the positive and negative directions, respectively. The positive and negative sequencing positions refer to the sequencing position of each cable when Br1 and Br8 fail, respectively. k is a positive integer from 0 to $\left|\phi_{\mathrm{Se}}\right|$, which represents the value of the cable sequencing position. For each cable (i, j), $w_{ij}^{k}=1$ indicates that the sequencing position is k in the positive direction, while $v_{ij}^{k}=1$ indicates that the sequence position is k in the negative direction. For cable Br3, w_{23}^{2} and v_{23}^{5} are equal to 1, while $w_{ij}^{k\neq 2}$ and $v_{ij}^{k\neq 5}$ are equal to 0. The maximum sequencing position of cable (2, 3) $L_{\mathrm{se},23}^{\max}$ is equal to 5, and the COR of cable (2, 3) is equal to 5 WTs. Therefore, each cable can match with its maximum sequencing position and meet the COR requirement. Equation (3) defines the number of the cable sequencing positions $\left|\phi_{\mathrm{Se}}\right|$. For example, if the capacity of a WT P^{WT} is 5 MW and the maximum cable rating $P_{\mathrm{Ca}}^{\max}$ is 39.4 MW, then $\left|\phi_{\mathrm{Se}}\right|$ is 7, which means that the cable with the maximum rating supports up to 7 WTs. Equation (4) indicates the expression of maximum sequencing position of each cable.

$$\sum_{(i,j)\in\phi_{\mathrm{L}}}\sum_{k=1}^{\left|\phi_{\mathrm{Se}}\right|}kw_{ij}^{k}-\sum_{(i,j)\in\phi_{\mathrm{L}}}\sum_{k=1}^{\left|\phi_{\mathrm{Se}}\right|}kw_{ji}^{k}=1 \tag{1}$$

$$\sum_{(i,j)\in\phi_{\mathrm{L}}}\sum_{k=1}^{\left|\phi_{\mathrm{Se}}\right|}kv_{ji}^{k}-\sum_{(i,j)\in\phi_{\mathrm{L}}}\sum_{k=1}^{\left|\phi_{\mathrm{Se}}\right|}kv_{ij}^{k}=1 \tag{2}$$

$$\left|\phi_{\mathrm{Se}}\right|=\left\lfloor P_{\mathrm{Ca}}^{\max}/P^{\mathrm{WT}}\right\rfloor \tag{3}$$

$$L_{\mathrm{se},ij}^{\max}=\sum_{k,h\in\phi_{\mathrm{Se}}}\max(k,h)w_{ij}^{k}v_{ij}^{h} \tag{4}$$

where ϕ_{Se} and ϕ_{L} are the sets of cable maximum sequencing positions and cables, respectively; $L_{\mathrm{se},ij}^{\max}$ is the maximum sequencing position of cable (i, j); and $\lfloor\cdot\rfloor$ denotes the lower bound.

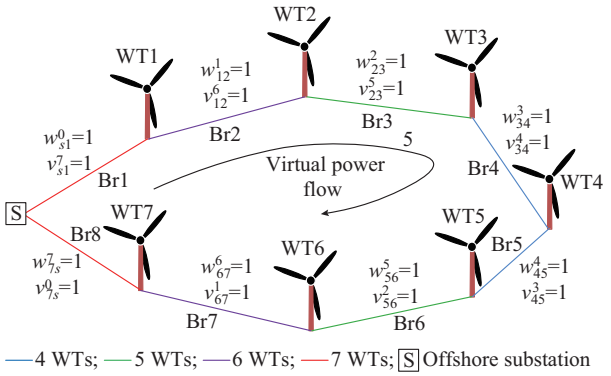

Fig. 3. Bidirectional flow conservation method.

IV. CSP Formulation

A. Cost Function

Define a weighted graph $G=(\phi_{\mathrm{N}}, \phi_{\mathrm{L}}, \phi_{\mathrm{Se}})$, where $\phi_{\mathrm{N}}=\{\phi_{\mathrm{S}}, \phi_{\mathrm{WT}}\}$, and ϕ_{N}, ϕ_{S}, ϕ_{WT} are the sets of nodes, substation nodes, and WT nodes, respectively. The total objective function of OWF-CS includes investment costs and operation costs. The constraints of the CSP problem include the CVRP, sequencing position, and 3D DC power flow constraints. The nonconvex nonlinear terms in the objective function and constraints are convexified to formulate the CSP problem into a standard MIQP function.

1) Objective 1: the first objective is to minimize the investment cost f_{inv}, which is a function of cable length and cable type.

$$f_{\mathrm{inv}}=\sum_{(i,j)\in\phi_{\mathrm{L}}}\left(\sum_{k,h\in\phi_{\mathrm{Se}}}w_{ij}^{k}v_{ij}^{h}c_{ij}^{\max(k,h)}\right)D_{ij}\quad\forall i,j\in\phi_{\mathrm{N}} \tag{5}$$

where $c_{ij}^{\max(k,h)}$ is the cost of cable (i, j) with the maximum sequencing position k or h; and D_{ij} is the distance of cable (i, j).

2) Objective 2: the second objective is to minimize the operation cost f_{loss}, which is the function of the power loss.

$$f_{\mathrm{loss}}=\sum_{(i,j)\in\phi_{\mathrm{L}}}\left(\sum_{k,h\in\phi_{\mathrm{Se}}}w_{ij}^{k}v_{ij}^{h}r_{ij}^{\max(k,h)}\right)P_{ij}^{2}D_{ij}\quad\forall i,j\in\phi_{\mathrm{N}} \tag{6}$$

where $r_{ij}^{\max(k,h)}$ is the resistance of cable (i, j) with the maximum sequencing position k or h; and P_{ij} is the power flow in cable (i, j). As the voltage amplitude of each node can be regarded as 1 p.u. in the CSP, the current of each cable is equal to the power, thus the power loss P_{ij}^{loss} can be approximately expressed as $r_{ij}P_{ij}^{2}$ [21].

By combining (5) and (6), the cost function is expressed as:

$$\min\left\{f_{\mathrm{inv}}+\sum_{t=1}^{T}\frac{1}{(1+r)^{t}}h^{\mathrm{year}}c_{\mathrm{loss}}f_{\mathrm{loss}}\right\} \tag{7}$$

where $c_{\mathrm{loss}}=120$ \$/MWh is the electricity price; $T=20$ years is the planning time period; $r=0.08$ is the discount rate; and $h^{\mathrm{year}}=8760$ is the total number of hours in a year.

B. Constraints

1) CVRP Constraints

The basic CVRP constraints are that each customer point must be visited only once, and the route of each vehicle must start at the depot and end at the depot. The CSP also needs to meet the above constraints.

$$\sum_{(s,i)\in\phi_{\mathrm{L}}}x_{si}=m\quad\forall i\in\phi_{\mathrm{WT}},\forall s\in\phi_{\mathrm{S}} \tag{8}$$

$$\sum_{(j,s)\in\phi_{\mathrm{L}}}x_{js}=m\quad\forall j\in\phi_{\mathrm{WT}},\forall s\in\phi_{\mathrm{S}} \tag{9}$$

where x_{ij} is the binary variable of cable (i, j); and m is the number of loops. Equations (8) and (9) represent that the numbers of outflow cables of substation node and the number of inflow cables of substation node are equal to m, respectively.

$$m\geq\left\lceil N^{\mathrm{WT}}/\left\lfloor P_{\mathrm{Ca}}^{\max}/P^{\mathrm{WT}}\right\rfloor\right\rceil \tag{10}$$

where N^{WT} is the total number of WTs; $P_{\mathrm{Ca}}^{\max}$ is the maximum rated power of all optional cables; and $\lceil\cdot\rceil$ denotes the upper bound. P^{WT} is obtained by a typical wind power case using the fuzzy c-means (FCM) algorithm. Equation (10) can improve the convergence by defining the minimum value of m. For example, the number of loops should not be less than 5 for an OWF comprising 30 WTs, each with a capacity of 5 MW and a maximum cable rating of 39.4 MW.

$$\sum_{(i,j)\in\phi_{\mathrm{L}}}x_{ij}=1\quad\forall i,j\in\phi_{\mathrm{WT}} \tag{11}$$

$$\sum_{(i,j)\in\phi_{\mathrm{L}}}x_{ji}=1\quad\forall i,j\in\phi_{\mathrm{WT}} \tag{12}$$

Equations (11) and (12) represent that the outflow and inflow cables of each WT node are equal to 1, respectively, to guarantee the ring topology of the CS.

$$u_i-u_j+1\leq\left\lfloor P_{\mathrm{Ca}}^{\max}/P^{\mathrm{WT}}\right\rfloor(1-x_{ij})\quad\forall i,j\in\phi_{\mathrm{N}} \tag{13}$$

where u_i is the order of WT i on the cable, with the transformer as the starting point. Equation (13) is known as the Miller-Tucker-Zemlin (MTZ) [30] formulation constraint to eliminate the subtours, which can also limit the number of WTs in a ring.

2) Cable Sequencing Constraints

The cable sequencing constraints (14)-(17) are the original constraints for CSP to ensure that each cable autonomously matches its maximum sequencing position and meet the COR requirement.

$$\text{(1), (2)} \tag{14}$$

$$\sum_{k\in\phi_{\mathrm{Se}}}w_{ij}^{k}=x_{ij}\quad\forall(i,j)\in\phi_{\mathrm{L}} \tag{15}$$

$$\sum_{k\in\phi_{\mathrm{Se}}}v_{ij}^{k}=x_{ij}\quad\forall(i,j)\in\phi_{\mathrm{L}} \tag{16}$$

$$\sum_{k,h\in\phi_{\mathrm{Se}}}w_{ij}^{k}v_{ij}^{h}=x_{ij}\quad\forall(i,j)\in\phi_{\mathrm{L}} \tag{17}$$

Equations (15) - (17) represent that if a cable exists be-

tween two WTs, then only one positive and negative sequencing position exists.

3) 3D DC Plow Flow Constraints

The DC power flow model has linearized the voltage phase angle with respect to the active power. The optimal power flow for minimizing the power losses can be directly solved based on the MIQP when considering the unified rating matching. However, the CSP with autonomous cable rating matching cannot be directly calculated by using the above method. The 3D DC power flow model for OWF is established as:

$$\text{(26)-(29)} \tag{18}$$

$$\theta_s = 0 \quad \forall s \in \phi_{\mathrm{S}} \tag{19}$$

$$\theta_{\min} \le \theta_i \le \theta_{\max} \quad \forall i \in \phi_{\mathrm{WT}} \tag{20}$$

where θ_i is the voltage phase angle of WT i. Equation (19) and (20) are the voltage phase angle constraints. Equation (19) denotes that the substation node is the slack node. Equation (20) denotes that the phase angle remains within a feasible range.

$$\sum_{(i,j)\in\phi_{\mathrm{L}}} P_{ij} = P_i^{\mathrm{WT}} + \alpha_i \quad \forall i,j \in \phi_{\mathrm{WT}} \tag{21}$$

$$\left| P_{ij} \right| \le M x_{ij} \quad \forall (i,j) \in \phi_{\mathrm{L}} \tag{22}$$

$$\left| \left(\sum_{k,h\in\phi_{\mathrm{Se}}} w_{ij}^k v_{ij}^h B_{ij}^{\max(k,h)} D_{ij} \right)(\theta_j - \theta_i) - P_{ij} \right| \le (1 - x_{ij}) M \quad \forall (i,j) \in \phi_{\mathrm{L}} \tag{23}$$

where $\alpha_i \in [0, 0.01]$ is the relaxing factor for the power balance at each WT node; M is a large number; and $B_{ij}^{\max(k,h)}$ is the conductance of cable (i, j) with the maximum sequencing position. Equations (21) and (22) are the constraints on the power collected on the cables. Equation (21) denotes the power balance at each WT node; (22) denotes that the power remains within a feasible range; and (23) defines the relationship between the voltage phase angle of WT and the active power collected in cable (i, j) ($x_{ij} = 1$) with the big-M method. If $x_{ij} = 0$, the active power is independent of the voltage phase angle.

C. Rationality Model of MV Cable Route

1) Cable Crossing-avoidance Constraints

Cables can be regarded as line segments. If two line segments intersect at any point other than their endpoints, the two cables have crossed. Assuming that x_{ij} and x_{mn} represent a set of crossing cable pairs (CCPs), the CCA constraint can be expressed as [20]:

$$x_{ij} + x_{ji} + x_{mn} + x_{nm} \le 1 \quad \forall (ij, mn) \in \phi_{\mathrm{CCP}} \tag{24}$$

where ϕ_{CCP} is the set of CCPs.

2) Cable Length Constraints

The maximum connection distance $D^{\max}$ is defined to limit the cable length between two WTs, e. g., cables crossing more than 3 WTs. The cable length constraints can be expressed as:

$$x_{ij} = 0 \quad \forall D_{ij} \ge D^{\max} \tag{25}$$

Figure 4 displays the route rationality model of the MV cable in the pre-deterministic stage. MV cables with length exceeding the maximum connection distance or those crossed with HV cables are considered non-candidate cables to reduce topological connection variables and save computational time.

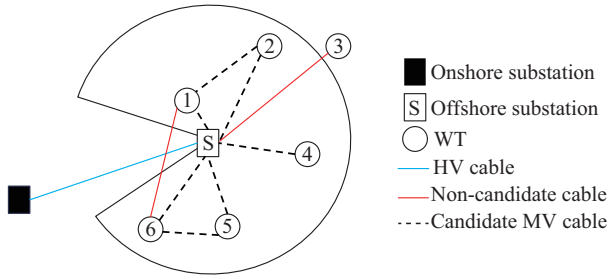

Fig. 4. Route rationality model of MV cable.

D. Wake Effect Model and Wind Power Calculation

The wake effect, originating from WT-atmosphere interactions, has long-term impacts on power loss and operation costs of the OWF [1]. The wake effect has been considered in some heuristic algorithms [10], [19], [31] to improve the applicability of CSP to the real-world OWF. The Jensen wake model is widely used to calculate the wind speed at each WT because it is fast and meets engineering accuracy requirements [32].

1) Jensen Wake Model

The Jensen wake model is described as:

$$\begin{bmatrix} X \\ Y \end{bmatrix} = \begin{bmatrix} \cos\theta^{\mathrm{WD}} & \sin\theta^{\mathrm{WD}} \\ -\sin\theta^{\mathrm{WD}} & \cos\theta^{\mathrm{WD}} \end{bmatrix} \begin{bmatrix} x \\ y \end{bmatrix} \tag{26}$$

$$v_{ij} = v_i \left[1 - \sqrt{1 - C_{t,i}} \left(1 + \frac{\alpha D_{ij}}{R} \right)^{-2} \frac{A_{\mathrm{s}}^{ij}}{A_0} \right] \quad \forall i,j \in \phi_{\mathrm{WT}} \tag{27}$$

$$v_j = \sqrt{v_0^2 - \sum_{j\in\Gamma_i} (v_i^2 - v_{ij}^2)} \quad \forall i,j \in \phi_{\mathrm{WT}} \tag{28}$$

where x and y are the coordinates in x-y plane; X and Y are the coordinates in X-Y plane; v_i is the wind speed of WT i; $C_{t,i}$ is the thrust coefficient of WT i; α is the wake expansion coefficient; R is the rotor radius of WT; $A_0 = \pi R^2$ is the rotor swept area; A_{s}^{ij} is the wake shadow area of WT i caused by WT j; θ^{WD} is the angle between x-axis and X-axis; Γ_i is the set of WTs that have wake effect on WT i; and v_0 is the freestream wind speed. Equation (26) decomposes a given wind direction into the X-axis and Y-axis; (27) describes the effect of WT i on the wind speed of WT j; and (28) denotes the wake superposition model. The wind speed of each downstream WT is affected by multiple upstream WTs.

2) Wind Power Calculation

$$P^{\mathrm{WT}}(v) = \begin{cases} 0 & v \le v_{in}, v > v_{out} \\ \dfrac{1}{2} \rho A_0 C_{p,\max} v^3 \eta & v_{in} < v \le v_r \\ P_r^{\mathrm{WT}} & v_r < v \le v_{out} \end{cases} \tag{29}$$

where v, v_{in}, v_r, and v_{out} are the current, cut-in, rated, and cut-out wind speeds of WTs, respectively; ρ, $C_{p,\max}$, and η are the air density, wind power utilization factor, and WT gener-

ator efficiency, respectively; and P^{WT} and P_r^{WT} are the output active power and rated active power of the WT, respectively. Equation (29) denotes the segmented wind power curve of a WT.

Based on the historical wind speed and direction data of the OWF, the output power of all WTs can be calculated using (26) - (29). To reduce computational burden, a typical wind power case is derived using a weighting method or the FCM algorithm as a proxy for calculating the output power of the WT over the service life of the OWF.

V. Model Convexification and Solution

After considering the COR requirements for CSP, the above optimization planning model includes one binary variable with another multiplication term of binary variable, accumulated multiple binary variables with a multiplication term of continuous variable, and even accumulated multiple binary variables with a quadratic multiplication term of continuous variable. Therefore, it is essential to implement the equivalence alternative methods to convexify the non-convex objective functions and constraints and guarantee the accuracy and solvability of the solution process.

A. Convexification of the Maximum Sequencing Position

The expression of the maximum sequencing position of cable related to the positive and negative sequencing position is nonlinear. Define a binary auxiliary variable $y_{ij}^{l}=w_{ij}^{k}v_{ij}^{h}$, which is the element of a 3D matrix with size of $(N^{\mathrm{S}}+N^{\mathrm{WT}})\times(N^{\mathrm{S}}+N^{\mathrm{WT}})\times N^{\mathrm{T}}$, where N^{S}, N^{WT}, and N^{T} are the numbers of substations, WTs, and cable types, respectivley.

$$\begin{cases} y_{ij}^{l}\le w_{ij}^{k} \\ y_{ij}^{l}\le v_{ij}^{h} \\ y_{ij}^{l}\ge w_{ij}^{k}+v_{ij}^{h}-1 \end{cases} \quad \forall k,h\in\phi_{\mathrm{Se}},\forall l\in\phi_{l} \tag{30}$$

$$\left|\left(\sum_{l\in\phi_{l},k,h\in\phi_{\mathrm{Se}}} y_{ij}^{l}B_{ij}^{\max(k,h)}D_{ij}\right)(\theta_j-\theta_i)-P_{ij}+\delta_{ij}^{l}\right|\le(1-x_{ij})M \quad \forall(i,j)\in\phi_{\mathrm{L}} \tag{31}$$

where ϕ_l and δ_{ij} are the auxiliary variable and the relaxing factor of cable (i, j) for the branch power flow equation. Equation (30) linearizes the multiplication term. Equations (5) and (17) can also be converted to a linear expression. Equation (23) is converted to (31). The CSP problem remains non-convex when considering the power loss over the service life of OWF.

B. Convexification of Power Loss

Since the resistance and conductance of the cable are related to the maximum sequencing position, the power loss is a quintic function of both the maximum sequencing position of the cable and the voltage phase angle of the WT. A straightforward approach is to introduce four new variables to successively transform the quintic function into a linear function. Nevertheless, this gives rise to circular nesting, which in turn leads to an excessive amount of modelling effort and computation time. In some cases, it may even render the problem intractable.

To address the above issues, we multiply both sides of (29) simultaneously by the square root of the cable resistance to derive (32) and (33).

$$\sqrt{P_{ij}^{\mathrm{loss}}}=\left(\sum_{k,h\in\phi_{\mathrm{Se}}} y_{ij}^{l}\sqrt{r_{ij}^{\max(k,h)}}\right)P_{ij} \tag{32}$$

$$\sqrt{P_{ij}^{\mathrm{loss}}}=\left(\sum_{k,h\in\phi_{\mathrm{Se}}} y_{ij}^{l}\sqrt{r_{ij}^{\max(k,h)}}\right)\left(\sum_{k,h\in\phi_{\mathrm{Se}}} y_{ij}^{l}B_{ij}^{\max(k,h)}D_{ij}\right)(\theta_j-\theta_i) \tag{33}$$

where $\sqrt{P^{\mathrm{loss}}}$ is an auxiliary continuous variable, denoting the square root of power loss.

The linear relationship between the square root of the power loss with respect to θ and y is established for each cable and its maximum sequencing position by:

$$\sqrt{r_{ij}^{\max(k,h)}}\,B_{ij}^{\max(k,h)}D_{ij}(\theta_j-\theta_i)-M(1-y_{ij}^{l})+\sigma_{ij}^{l}\le\sqrt{P_{ij}^{\mathrm{loss}}}\le\sqrt{r_{ij}^{\max(k,h)}}\,B_{ij}^{\max(k,h)}D_{ij}(\theta_j-\theta_i)+M(1-y_{ij}^{l})+\sigma_{ij}^{l} \tag{34}$$

where σ_{ij} is the relaxing factor of cable (i, j) for the square root of the branch power loss equation.

C. Solution Method for CSP

The convexified objective function can be expressed as:

$$f_{\mathrm{inv}}=\sum_{(i,j)\in\phi_{\mathrm{L}}}\left(\sum_{k,h\in\phi_{\mathrm{Se}}} y_{ij}^{l}c_{ij}^{\max(k,h)}\right)D_{ij} \quad \forall i,j\in\phi_{\mathrm{N}},\forall l\in\phi_{l} \tag{35}$$

$$f_{\mathrm{loss}}=\sum_{(i,j)\in\phi_{\mathrm{L}}}\left(\sqrt{P_{ij}^{\mathrm{loss}}}\right)^{2} \quad \forall i,j\in\phi_{\mathrm{N}} \tag{36}$$

$$f_{\mathrm{rel}}=M\sum(\delta_{ij}^{l}+\sigma_{ij}^{l}) \quad \forall i\in\phi_{\mathrm{WT}},(i,j)\in\phi_{\mathrm{L}},l\in\phi_{l} \tag{37}$$

Equations (35) and (36) represent the convexified investment cost and convexified operation cost, respectively.

Therefore, the compact form of the CSP solution method can be expressed as:

$$\min\{(7),\ (35)\text{-}(37)\} \tag{38}$$

s.t.

$$(8)\text{-}(22),\ (24)\text{-}(25),\ (30)\text{-}(34) \tag{39}$$

The MIQP model can be solved by using the mathematical program solver Gurobi [33].

D. Reliability Assessment for Radial Topology

In a radial topology, if a submarine cable fails, all the WTs located downstream will be cut off from the grid. As a result, it is necessary to factor in reliability indicators when dealing with a radial network. The reliability of a radial topology is also assessed by computing the cost of the expected energy not generated (EENG). This computation takes into account the probability of outages and the mean time to repair (MTTR) of the submarine cable, which can be defined as:

$$f_{EENG}=c_{\mathrm{loss}}\cdot MTTR\cdot T\cdot fr\cdot\sum_{(i,j)\in\phi_{\mathrm{L}}} D_{ij}x_{ij}P_{ij} \quad \forall i,j\in\phi_{\mathrm{N}} \tag{40}$$

where f_{EENG} is the cost of EENG; $MTTR=1440$ is the mean time to repair; T is the service life of OWF; and $fr=0.00917$ is the failure rate of submarine cables in the OWF.

E. Verification and Calculation of Short-circuit Current

There are two reasons for the significant increase in current during the fault. ① The reactive power is injected from WTs. ② The equivalent impedance between the short-circuit point and the power source will decrease. Therefore, it is of great significance to consider the short-circuit current in fault scenarios [34].

Equation (41) takes into account the increase in the output current of the WTs and is used to calculate the voltage at the WT nodes after the fault. Equation (42) is used to calculate the increased current output of the WTs after the fault. First, define the increment of the output current of all WTs as 0, substitute it into (41), and then substitute the node voltage solved by (41) into (42). Keep iterating until the voltage difference calculated by the voltages of the two consecutive iterations is less than 0.001. Substitute the converged current increment into (43), and the short-circuit current can be calculated.

$$U_{(1)\mathrm{kW}j}=\frac{U_{\mathrm{kW}_0 j}}{\sqrt{3}}-Z_{ij}\left(\frac{cU_{\mathrm{n}}}{\sqrt{3}\,Z_{ii}}+\frac{1}{Z_{ii}}\sum_{j\in\phi_{\mathrm{WT}}}Z_{ij}\Delta I_{(1)\mathrm{kW}j}\right)+\sum_{m\in\phi_{\mathrm{WT}}}Z_{mj}\Delta I_{(1)\mathrm{kW}m} \tag{41}$$

$$\begin{cases}\Delta\dot{I}_{(1)\mathrm{kW}}=\begin{cases}0 & U_{(1)\mathrm{kW}}\geq U_{\mathrm{L1}}\\ \left(I_{(1)d\mathrm{ref}}-\dfrac{P_{\mathrm{ref0}}I_{\mathrm{N}}}{S_{\mathrm{N}}}\right)+\mathrm{j}\left(\dfrac{Q_{\mathrm{ref0}}I_{\mathrm{N}}}{S_{\mathrm{N}}}-I_{(1)q\mathrm{ref}}\right) & U_{(1)\mathrm{kW}}<U_{\mathrm{L1}}\end{cases}\\ I_{(1)q\mathrm{ref}}=\min\left\{\left|-\dfrac{Q_{\mathrm{ref0}}}{S_{\mathrm{N}}}I_{\mathrm{N}}-\dfrac{K_{(1)\mathrm{L}}(U_{\mathrm{L2}}-U_{(1)\mathrm{kW}})}{U_{\mathrm{N}}}I_{\mathrm{N}}\right|,I_{\max}\right\}\\ I_{(1)d\mathrm{ref}}=\min\left\{\dfrac{P_{\mathrm{ref0}}}{S_{\mathrm{N}}}I_{\mathrm{N}},\sqrt{I_{\max}^2-I_{(1)q\mathrm{ref}}^2}\right\}\end{cases} \tag{42}$$

$$I_k=\sqrt{3}\left(\frac{1.5U_{\mathrm{n}}}{\sqrt{3}\,Z_{ii}}+\frac{1}{Z_{ii}}\sum_{j\in\phi_{\mathrm{WT}}}Z_{ij}\Delta I_{(1)\mathrm{kW}j}\right) \tag{43}$$

where c is the voltage coefficient; $U_{(1)\mathrm{kW}j}$ and $U_{\mathrm{kW}_0 j}$ are the voltage magnitudes of the j^{th} WT after and before the fault, respectively; $U_{(1)\mathrm{kW}}$ is the voltage magnitude after the fault; U_{n} is the rated voltage; Z_{ij} is the magnitude of the element in the i^{th} row and j^{th} column of the nodal impedance matrix; $\Delta I_{(1)\mathrm{kW}j}$ is the positive-sequence current increment magnitude of the j^{th} WT before and after the fault; $\Delta\dot{I}_{(1)\mathrm{kW}}$ is the positive-sequence current increment before and after the fault; P_{ref0} and Q_{ref0} are the reference values of the active and reactive power output before the fault, respectively; $K_{(1)\mathrm{L}}$ is the positive-sequence reactive current coefficient, usually with a value range of 1.0-3.0; U_{L1} and U_{L2} are the voltage thresholds for entering the low voltage ride-through control state and the voltage reference value for calculating the low voltage ride-through reactive current, respectively, usually taken as 0.9 times the rated voltage; S_{N} and I_{N} are the rated capacity and current of the WT, respectively; $I_{(1)d\mathrm{ref}}$ and $I_{(1)q\mathrm{ref}}$ are the reference values of the post-fault d- and q-axis positive-sequence currents, respectively; $I_{\max}$ is the maximum allowable output current value; and I_k is the short-circuit current.

VI. Case Study

A. Test Systems

The OWF-CS is implemented using Gurobi and MATLAB R2019a with an Intel Core i7-12700F 2.10 GHz CPU and 32 GB RAM processor. Three test systems, namely 20-, 30-, and 42-WT OWFs, are derived by adapting the Saint-Brieuc OWF [35]. The real historical wind rose diagram in 2023 at Cape San Martin (55 NM West NW of Morro Bay) is depicted in Fig. 5, where the abbreviations such as N, NNE, and NE around the circle indicate the 16 wind directions; and the percentile values indicate the frequency of wind speed. Table I describes the detailed steps of CSP solution method.

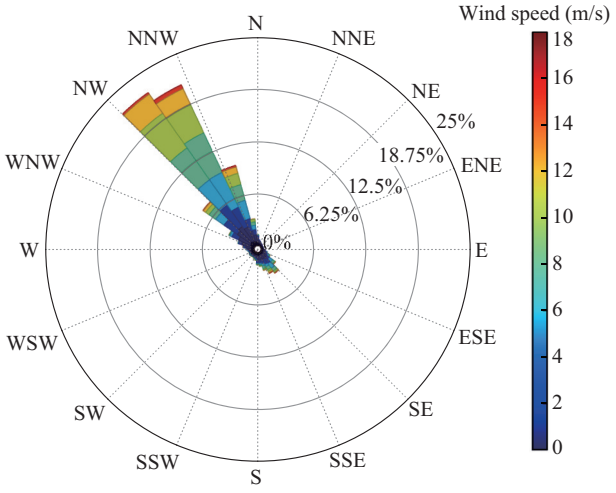

Fig. 5. Wind rose diagram in 2023 at Cape San Martin.

Table II outlines the specifications of 33 kV aluminum cross linked polyethylene (XLPE) cables, including cross-sectional areas ranging from 70 to 630 mm² and their corresponding rated capacity, resistance, inductance, and cost [36]. The thrust coefficient of each WT $C_{t,i}$, wake expansion coefficient α, air density ρ, wind power utilization factor $C_{p\max}$, and WT generator efficiency η are set to be 0.8, 0.04, 1.2231 kg/m^3, 0.46, and 0.0944, respectively. Table III displays the parameters of WTs with capacities of 5 MW and 6.25 MW [37]. The base voltage is 33 kV, and the base power is set according to the WT capacity.

B. Comparison Analysis of Different Planning Methods

Three cases are used to compare different planning methods. In Cases a-c, the OWF-CS test systems with 20, 30, and 42 WTs are used. Four different planning methods are used: ① MIQP method to construct the radial topology, ② sweep + Clark and Wright saving algorithm (CW) [19] and ant colony optimization (ACO) [38] (CW/ACO) method, ③ CSP with unified rating requirements (method without COR), and ④ the proposed optimal CSP method.

The sweep algorithm divides the WTs into clusters counterclockwise from the direction of the HV cable to prevent cable crossings [19]. CW and ACO are heuristic for solving the VPR problem and are applied to CSP. The method without COR [21] is also compared with the proposed optimal CSP method.

TABLE I
DETAILED STEPS OF CSP SOLUTION METHOD

Step	Description
Step 1	Initialize: acquire information about the offshore substation location, location of HV cables, WT locations, WT capacities, cable types, and the wind rose diagram of the OWF. Use a binary varaible *cross_cable* = 1 to indicate cable crossing.
Step 2	Calculate the wind speed at each WT using the wake model and the wind rose diagrams. Employ the FCM algorithm to obtain a typical wind scenario, which serves as a substitute for calculating the WT output power throughout the service life of OWF.
Step 3	**while** *cross_cable* = 1 **do**
Step 4	Define reference power, reference voltage, and cable length constraints. Define binary variables such as x, w, v, integer variables such as u, m, and continuous variables such as P, θ.
Step 5	Calculate the distance matrix and the node conductance matrix. Reduce the topological connection variables in the pre-deterministic stage.
Step 6	In the computational stage, the optimization result can be obtained based on the MIQP with the objective (38) and constraint (39).

Step 7	**if** no cable crossing situation in verification stage and the verification of the short-circuit current is successful **then**
	cross_cable = 0
	Output the optimal topology, investment, and operation costs.
	else
	Add the constraints of cable crossing situation to computational stage.
	end if

Step 8	**end while**

TABLE II
SPECIFICATIONS OF 33 KV ALUMINUM XLPE CABLES

Cross-sectional area (mm^2)	0.5 s short current (kA)	Rated capacity (MVA)	R (Ω/km)	X (Ω/km)	Cost ($/m)
70 (3-core MV)	9.35	11.1	0.568	0.129	64
95 (3-core MV)	12.70	13.1	0.410	0.122	71
150 (3-core MV)	20.04	16.6	0.265	0.114	87
185(3-core MV)	24.72	18.9	0.211	0.110	96
240 (3-core MV)	32.07	21.7	0.161	0.106	103
300 (3-core MV)	40.08	24.3	0.129	0.102	109
400 (3-core MV)	53.44	27.4	0.102	0.098	114
500 (single-core MV)	66.81	34.9	0.080	0.104	121
630 (single-core MV)	84.17	39.4	0.063	0.100	131

TABLE III
PARAMETERS OF WT WITH CAPACITIES OF 5 MW AND 6.25 MW

WT capacity (MVA)	Rotor radius (m)	v_{in} (m/s)	v_r (m/s)	v_{out} (m/s)
5.00	63.0	3.0	11.4	25
6.25	85.5	2.5	10.2	24

Table IV displays the economic comparison of OWF-CS test systems with 20, 30, and 42 WTs. The radial topology constructed by MIQP method features a simple and straightforward connection pattern. Although the investment costs of the radial topology account for only 45%-48% of those of the ring topology, the radial topology incurs higher operation costs and also generates the EENG costs. In the OWF-CS test systems with 20, 30, and 42 WTs, the total cost of the radial topology is 1.9%, 3.9%, and 25.9% higher than those of the ring topology, respectively. As the scale of the test system increases, the advantages of the ring topology become more prominent. This is because cable failures will have a greater impact on the wind farm. The costs of CW and ACO are the same, with CW having a shorter solution time. Compared with the two heuristic methods, the investment costs of the proposed optimal CSP method are saved by 9.92%, 9.40%, and 2.37% for the test systems with 20, 30, and 42 WTs, respectively; and the total costs of the proposed optimal CSP method are saved by 9.45%, 8.89%, and 1.76%. The economic similarity between the proposed optimal CSP method and the two heuristic methods in the OWF-CS test system with 42 WTs can be attributed to its superior effectiveness of sweep partitioning. Compared with the method without COR, the investment costs of proposed optimal CSP method are saved by 18.57%, 13.55%, and 9.27% for the test systems with 20, 30 and 42 WTs, respectively. The proposed method outperforms heuristic methods and the method without COR in terms of investment costs and total costs. Although the proposed method has a longer calculation time, it is acceptable for the CSP problem. The gap for test system with 20 WTs is 0, indicating that a globally optimal solution is determined to be found. The gaps for 30 and 42 WTs are 4.72% and 7.21%, respectively. It is worth mentioning that even if the gap is not 0, the solution may be globally optimal.

TABLE IV
ECONOMIC COMPARISON OF OWF-CS TEST SYSTEMS WITH 20, 30, AND 42 WTS

Number of WTs	Method	Investment cost (k$)	Operation cost (k$)	EENG (k$)	Total cost (k$)
20	MIQP	868.8	346.5	546.0	1761.26
	Sweep + CW/ACO	1780.8	103.4	0	1884.24
	Without COR	1969.9	79.6	0	2049.47
	Proposed	1604.1	102.1	0	1706.17
30	MIQP	1774.9	760.5	1185.1	3720.49
	Sweep + CW/ACO	3691.3	233.5	0	3924.78
	Without COR	3868.4	189.3	0	4057.72
	Proposed	3330.7	238.9	0	3569.60
42	MIQP	4660.7	3929.2	5080.3	13670.20
	Sweep + CW/ACO	9151.6	1158.9	0	10310.50
	Without COR	9847.3	1052.1	0	10899.40
	Proposed	8934.8	1194.6	0	10129.40

Figure 6 displays the planning topology results using different methods. The maximum connection distances $D^{\max}$ of OWF-CS test systems with 20, 30, and 42 WTs are 1.5 km, 1.7 km, and 4.0 km, respectively. The WT capacities of OWFs with 20, 30, 42 WTs are 5 MW, 5 MW, and 6.25 MW, respectively. The characteristics of the MIQP method lie in that the connection method is simple and straightforward, and the required cross-sectional area of the cables is relatively smaller. The ring topology has enough redundancy. Even if a certain section of the cable fails, electricity can still be transmitted through other parts. By comparing the to-

pologies among the three test systems, it can be observed that the test system with 42 WTs has the highest similarity and the most effective sweep partitioning. The sweep partitions of WTs 18, 26, 35, 24, and 37 deviate from the proposed optimal CSP method. In the OWF with 42 WFs, since the total number of WTs in the OWF is divisible by the maximum number of WTs that a feeder can accommodate, the topological results obtained by the sweep method and the proposed method are similar. Additionally, there are no instances of excessively long cables as observed in the test system with 20 WTs with the cable S-WT5 or the test system with 30 WTs with the cable WT21-WT25.

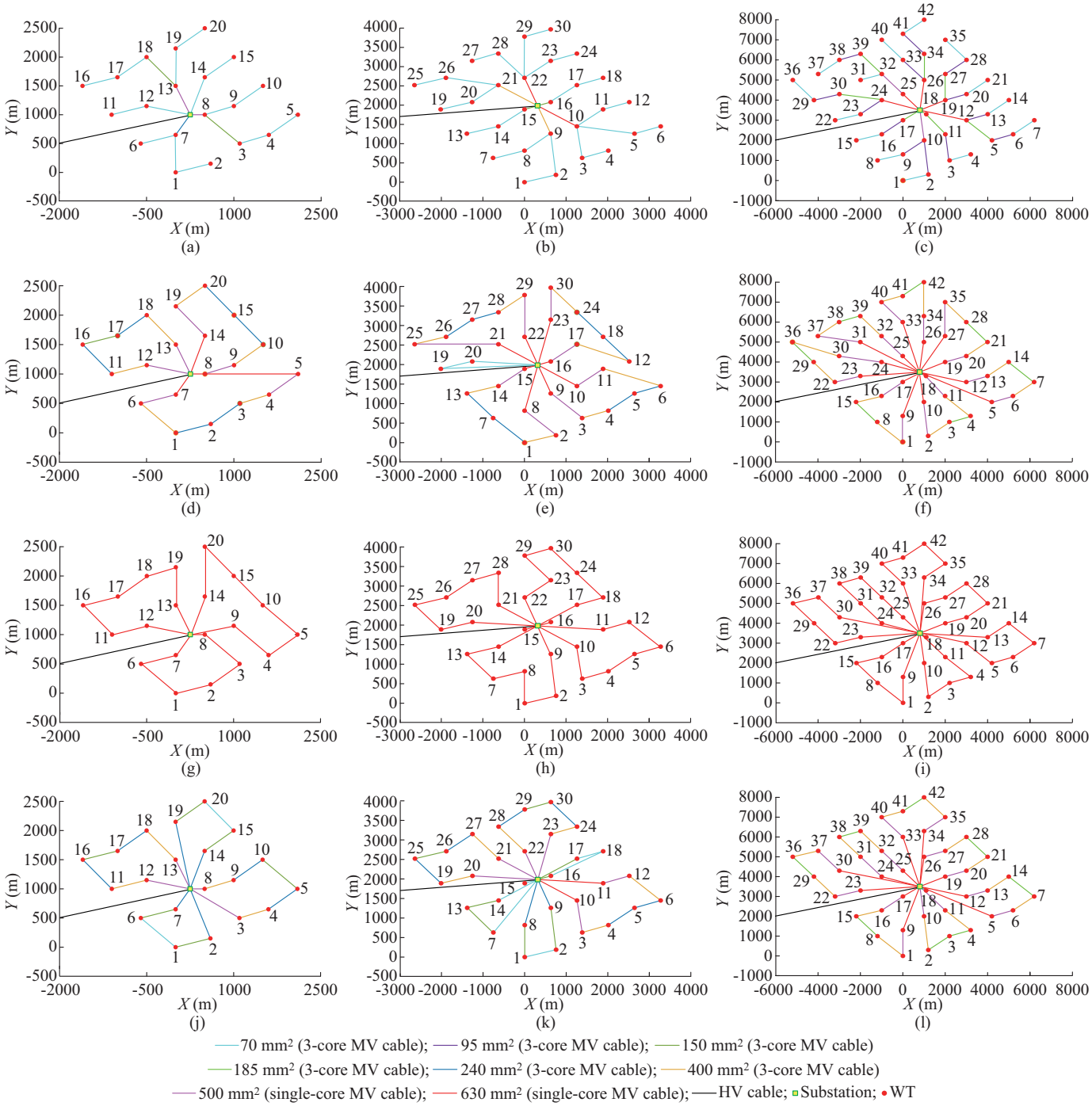

Fig. 6. Planning topology results obtained using different methods. (a) 20 WTs using MIQP method. (b) 30 WTs using MIQP method. (c) 42 WTs using MIQP method. (d) 20 WTs using sweep + CW/ACO method. (e) 30 WTs using sweep + CW/ACO method. (f) 42 WTs using sweep + CW/ACO method. (g) 20 WTs using method without COR. (h) 30 WTs using method without COR. (i) 42 WTs using method without COR. (j) 20 WTs using proposed optimal CSP method. (k) 30 WTs OWF using proposed optimal CSP method. (l) 42 WTs using proposed optimal CSP method.

C. Discussion on Power Loss Function

The topology with 20 WTs without considering power loss (refered to as "method without loss") is shown in Fig. 7. The investment and operation costs of the proposed optimal CSP method in OWF-CS test system with 20 WTs are 1602.1 k$ and 114.28 k$, respectively. Although the invest-

ment costs of the proposed optimal CSP method are higher by 0.12% than the method without loss in the OWF-CS test system with 20 WTs, the total cost of the proposed optimal CSP method is saved by 0.59%. The topology and costs for the OWF-CS test systems with 30 and 42 WTs using the method without loss are the same as those obtained using the proposed optimal CSP method, as shown in Fig. 6(f) and (i). Consequently, topology diagrams are not presented. The computation time of the proposed optimal CSP method in OWF-CS test systems with 20, 30, 42 WTs are 29987 s, 36000 s, 54000 s, respectively.

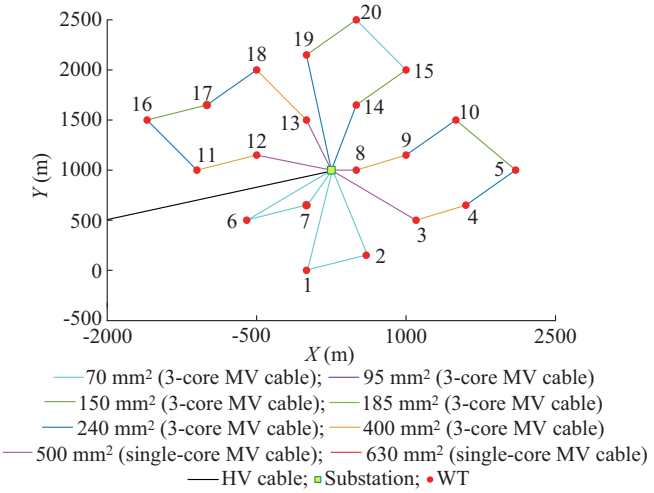

Fig. 7. Topology of OWF-CS test system with 20 WTs using method without loss.

However, the computation time of the method without loss in OWF-CS test systems with 20, 30, and 42 WTs are 81.6 s, 292.9 s, and 2553.9 s, respectively. The gaps in OWF-CS test systems with 20, 30, and 42 WTs are 0. The investment and operation costs are not inherently antagonistic. An escalation in one does not inexorably result in a diminution of the other. It is essential to conduct a comprehensive assessment of the proportion of operation costs to total costs, the required computation time, and the required computational accuracy to determine whether to include or exclude the quadratic term of network losses.

D. Results of Verification Stage

The voltage of the HV cable is 132 kV, and the distance from the shore is 20 km. The resistance and the reactance of the cable are 0.0212 Ω/km and 0.117 Ω/km, respectively [37]. The positive-sequence reactive current coefficient $K_{(i)L}$ is set to be 1.5. The maximum allowable output current I_{max} is set to be 1.5. U_{L1} and U_{L2} are both set to be 0.9. In the OWF-CS test systems with 20, 30, and 42 WTs, assuming that a three-phase-to-ground short circuit occurs, the short-circuit current is calculated. The results show that when the short circuit occurs at cable S8, S15, and S17, respectively, the short-circuit currents are the largest, and the maximum short-circuit currents are 5.03, 4.98, and 4.71 kA, respectively. There is an inverse relationship between cable length and short-circuit current. A shorter cable has lower resistance, which results in a higher magnitude of the short-circuit current of the cable. The currents of all cables during the short circuit do not exceed their rated short-circuit currents. Therefore, as long as the circuit breaker ensures that the faulty cable is cut off within 0.5 s [15], the above three systems will be able to successfully ride through the fault.

E. Approximation Error of Power Losses

In the realm of OWF-CSP, the linear DC flow model is used to calculate network losses, which may not be sufficiently accurate. The effectiveness and accuracy of the DC power flow model in calculating network losses need to be evaluated. The non-convexity AC power flow model is formulated in MATPOWER [39], with the reactive power from all WTs set to be zero. Then, the calculation errors of operation costs between the proposed optimal CSP method and the benchmark are compared. The results are presented in Table V.

TABLE V
CALCULATION ERRORS OF OPERATION COSTS BETWEEN PROPOSED OPTIMAL CSP METHOD AND BENCHMARK

Number of WTs	Operation cost (k$)		Error (%)
	Proposed	Benchmark	
20	103.1	102.1	1.01
30	227.3	231.5	1.79
42	1192.2	1194.6	0.20

When the DC power flow model is employed in the proposed optimal CSP method, and the approximated operation costs are incorporated into the objective function, the errors in operation costs for the OWF-CS test systems with 20, 30, and 42 WTs are determined to be 1.01%, 1.79%, and 0.20%, respectively. Such minimal error values are considered negligible in the planning stage. Considering that the non-convexity of the AC power flow model and the associated computational burden in the optimization process are taken into account, the DC power flow model is reasonably adopted in the CSP.

F. Economic Results with Fully Linear AC Power Flow Model

The fully linear AC power flow is often applied in the operation stage after the planning. Compared with the method based on the DC power flow, using the fully linear AC power flow model can obtain more accurate total transfer capability values to evaluate the reliability of power transactions [40]. In the subsequent safety operations of the wind farm, the grid code requirements for reactive power need to be met. Therefore, the results of the fully linear AC power flow equations are supplemented and discussed. In the model, the influences of both active power and reactive power on the voltage magnitude and phase angle are taken into account. After the fully AC power flow equations for the planning of OWF-CSs are established, the model is convexified to linearize the calculation expressions of network losses in the same way as the convexification method for the DC power flow model, and this problem is also transformed into an MIQP problem.

The results of the MIQP problem based on the fully linear AC power flow model for the OWF-CS test systems with 20, 30, and 42 WTs after running for 36000 s are obtained,

as shown in Table VI. The power factor is set to be 0.95. For the OWF-CS test systems with 20 WTs, the investment cost is the same as that of the proposed optimal CSP method. Since the reactive power output of the WTs is also taken into account, the cable current and network losses will increase. For the OWF-CS test systems with 30 and 42 WTs, due to the excessive complexity of the calculation problems, it is obvious that the global optimal solutions have not been obtained, and the investment costs are higher than those of the proposed optimal CSP method. Among them, the optimal gap for the OWF-CS test system with 42 WTs is 46.75%, which indicates that an immeasurable amount of time is required to reach the global optimal solution. Therefore, in the case of planning problems for small-scale OWF-CS test system with sufficient calculation time, the fully linear AC power flow model can be adopted for more accurate calculations. However, as the scale of the OWF-CS test system expands, it is supported to use the DC power flow model.

TABLE VI
ECONOMIC RESULTS WITH FULLY LINEAR AC POWER FLOW MODEL

Number of WTs	Total cost (k$)	Investment cost (k$)	Operation cost (k$)	Gap (%)
20	1731.2	1604.1	127.2	7.31
30	3636.8	3376.4	260.4	9.66
42	16714.0	14580.0	2133.7	46.75

G. Evaluation of Expected Service Life

To make the paper applicable in the real world, the Monte Carlo method is used to provide a reasonable estimation on the expected service life of OWF-CS without replacing cables. The failure rate of submarine cables is set to be 0.0045 time/(km·year). Since an OWF-CS with double-ring topology can still operate normally when only one cable on the ring fails, the wind farm is considered to have reached its expected service life when two cables on the ring fail.

Table VII displays the evaluation results of expected service life of the OWF-CS test systems with 20, 30, and 42 WTs. Each OWF-CS test system has undergone 10000 simulations, and the service life of an OWF-CS is set to be 20 years. Without considering cable replacement, in the test systems with 20, 30, and 42 WTs, the wind farms reach their expected service life in 1646, 3761, and 8612 cases, respectively. The year when the wind farm reaches its expected service life is recorded. For the wind farms that do not reach their expected service life, their service life is assumed to be 20 years. By taking the average of the 10000 simulations, the simulated average expected service lives are 18.93 years, 17.28 years, and 12.00 years, respectively.

TABLE VII
EVALUATION RESULTS OF EXPECTED SERVICE LIFE

Number of WTs	Number of loops	Number of failures	Average expected service life (year)	Proportion (%)
20	4	1646	18.93	94.67
30	6	3761	17.28	86.39
42	8	8612	12.00	60.02

VII. CONCLUSION

This paper proposes the optimal CSP method in OWFs based on a bidirectional flow conservation method which aims at minimizing cable costs and total power losses while considering the COR requirements. Case studies yield four key conclusions.

1) The autonomous cable matching method outperforms heuristic methods in terms of investment cost and total cost, and guarantees a globally optimal solution for the OWF with 20 WTs. The investment costs of the proposed optimal CSP method are saved by 2.37%-9.92%. The total costs of the proposed optimal CSP method are saved by 1.76%-9.45%.

2) The COR requirements are proven to be more cost-effective in both investment and total costs compared with unified redundancy requirements. The investment and total cost savings decrease with the system size. The investment costs of proposed optimal CSP method are saved by 9.27%-18.57%. The total costs of the proposed optimal CSP method are saved by 7.06%-16.75%.

3) In the OWF-CS test system with 20 WTs, the solution time of the method without COR is shorter than that without loss. However, in the OWF-CS test systems with 30 and 42 WTs, the solution time of the method without COR is longer than that without loss. It shows that as the system grows, the quadratic term of network loss becomes the primary factor that influences the solution difficulty.

4) In OWF-CS test systems with 30 and 42 WTs, topologies obtained with and without loss remain the same, yet the solution time varies significantly. Hence, the quadratic term of network loss can be either retained or discarded in the CSP stage based on actual needs.

REFERENCES

[1] P. Veers, K. Dykes, E. Lantz *et al*., "Grand challenges in the science of wind energy," *Science*, vol. 366, no. 6464, pp. 2027-2036, Oct. 2019.
[2] D. Xu, A. Hu, C. S. Lam *et al*., "Cooperative planning of multi-energy system and carbon capture, utilization and storage," *IEEE Transactions on Sustainable Energy*, vol. 15, no. 4, pp. 2718-2732, Oct. 2024.
[3] B. Yang, B. Liu, H. Zhou *et al*., "A critical survey of technologies of large offshore wind farm integration: summary, advances, and perspectives," *Protection and Control of Modern Power Systems*, vol. 7, no. 1, p. 17, May 2022.
[4] Global Wind Energy Council. (2024, Dec.). Global Wind Report 2024. [Online]. Available: https://gwec.net/global-wind-report-2024/
[5] S. Wei, H. Wang, Y. Fu *et al*., "Electrical system planning of large-scale offshore wind farm based on $N+$ design considering optimization of upper power limits of wind turbines," *Journal of Modern Power Systems and Clean Energy*, vol. 11, no. 6, pp. 1784-1794, Nov. 2023.
[6] T. Zuo, Y. Zhang, X. Xie *et al*., "A review of optimization technologies for large-scale wind farm planning with practical and prospective concerns," *IEEE Transactions on Industrial Informatics*, vol. 19, no. 7, pp. 7862-7875, Jul. 2023.
[7] X. Ding, X. Shen, Q. Wu *et al*., "Smart switch configuration and reliability assessment method for electrical collector systems in offshore wind farms," *Journal of Modern Power Systems and Clean Energy*, vol. 12, no. 6, pp. 1773-1785, Nov. 2024.
[8] D. Song, J. Yan, Y. Gao *et al*., "Optimization of floating wind farm power collection system using a novel two-layer hybrid method," *Applied Energy*, vol. 348, p. 121546, Oct. 2023.
[9] S. Dutta and T. J. Overbye, "Optimal wind farm collector system topology design considering total trenching length," *IEEE Transactions on Sustainable Energy*, vol. 3, no. 3, pp. 339-348, Jul. 2012.
[10] S. Tao, Q. Xu, A. Feijóo *et al*., "Joint optimization of wind turbine micrositing and cabling in an offshore wind farm," *IEEE Transactions on Smart Grid*, vol. 12, no. 1, pp. 834-844, Jan. 2021.
[11] Y. Chen, Z. Y. Dong, K. Meng *et al*., "Collector system layout optimiza-

tion framework for large-scale offshore wind farms," *IEEE Transactions on Sustainable Energy*, vol. 7, no. 4, pp. 1398-1407, Oct. 2016.
[12] IBM. (2024, Dec.). IBM documentation. [Online]. Available: https://www.ibm.com/docs/www.ibm.com/docs/en
[13] J. A. Pérez-Rúa, M. Stolpe, K. Das *et al*., "Global optimization of offshore wind farm collection systems," *IEEE Transactions on Power Systems*, vol. 35, no. 3, pp. 2256-2267, May 2020.
[14] J. A. Pérez-Rúa, M. Stolpe, and N. A. Cutululis, "Integrated global optimization model for electrical cables in offshore wind farms," *IEEE Transactions on Sustainable Energy*, vol. 11, no. 3, pp. 1965-1974, Oct. 2019.
[15] J. Wei, S. Wang, S. Huang *et al*., "Optimal post-fault recovery control based on topology reconfiguration of wind farm collection systems," *IEEE Transactions on Industry Applications*, vol. 60, no. 2, pp. 3664-3675, Mar. 2024.
[16] C. S. Seo, S. H. Park, J. S. Lee *et al*., "Offshore wind power planning in Korea," in *Proceedings of 2013 15th European Conference on Power Electronics and Applications*, Lille, France, Sept. 2013, pp. 1-6.
[17] X. Gong, S. Kuenzel, and B. C. Pal, "Optimal wind farm cabling," *IEEE Transactions on Sustainable Energy*, vol. 9, no. 3, pp. 1126-1136, Jul. 2018.
[18] S. Wei, L. Zhang, Y. Xu *et al*., "Hierarchical optimization for the double-sided ring structure of the collector system planning of large offshore wind farms," *IEEE Transactions on Sustainable Energy*, vol. 8, no. 3, pp. 1029-1039, Jul. 2017.
[19] T. Zuo, Y. Zhang, K. Meng *et al*., "Collector system topology for large-scale offshore wind farms considering cross-substation incorporation," *IEEE Transactions on Sustainable Energy*, vol. 11, no. 3, pp. 1601-1611, Jul. 2020.
[20] T. Zuo, Y. Zhang, K. Meng *et al*., "A two-layer hybrid optimization approach for large-scale offshore wind farm collector system planning," *IEEE Transactions on Industrial Informatics*, vol. 17, no. 11, pp. 7433-7444, Nov. 2021.
[21] X. Shen, Q. Wu, H. Zhang *et al*., "Optimal planning for electrical collector system of offshore wind farm with double-sided ring topology," *IEEE Transactions on Sustainable Energy*, vol. 14, no. 3, pp. 1624-1633, Jul. 2023.
[22] M. Banzo and A. Ramos, "Stochastic optimization model for electric power system planning of offshore wind farms," *IEEE Transactions on Power Systems*, vol. 26, no. 3, pp. 1338-1348, Aug. 2011.
[23] X. Ding, Y. Du, X. Shen *et al*., "Reliability-based planning of cable layout for offshore wind farm electrical collector system considering post-fault network reconfiguration," *IEEE Transactions on Sustainable Energy*, vol. 16, no. 1, pp. 419-433, Jan. 2025.
[24] J. A. Pérez-Rúa, S. Lumbreras, A. Ramos *et al*., "Reliability-based topology optimization for offshore wind farm collection system," *Wind Energy*, vol. 25, no. 1, pp. 52-70, Jan. 2022.
[25] R. Fukasawa and J. Gunter, "The complexity of branch-and-price algorithms for the capacitated vehicle routing problem with stochastic demands," *Operations Research Letters*, vol. 51, no. 1, pp. 11-16, Jan. 2023.
[26] O. Dahmani, S. Bourguet, M. Machmoum *et al*., "Optimization of the connection topology of an offshore wind farm network," *IEEE Systems Journal*, vol. 9, no. 4, pp. 1519-1528, Dec. 2015.
[27] M. Lavorato, J. F. Franco, M. J. Rider *et al*., "Imposing radiality constraints in distribution system optimization problems," *IEEE Transactions on Power Systems*, vol. 27, no. 1, pp. 172-180, Feb. 2012.
[28] Y. Wang, Y. Xu, J. Li *et al*., "On the radiality constraints for distribution system restoration and reconfiguration problems," *IEEE Transactions on Power Systems*, vol. 35, no. 4, pp. 3294-3296, Apr. 2020.
[29] A. Wędzik, M. Szypowski, and T. Siewierski, "An integrated method to simultaneously optimise a wind farm's internal network layout, cable cross-sections and substation location," *Applied Energy*, vol. 377, p. 124361, Jan. 2025.
[30] C. E. Miller, A. W. Tucker, and R. A. Zemlin, "Integer programming formulation of traveling salesman problems," *Journal of the ACM*, vol. 7, no. 4, pp. 326-329, Oct. 1960.
[31] Y. Fu, Y. Liu, L. Huang *et al*., "Collection system topology for deep-sea offshore wind farms considering wind characteristics," *IEEE Transactions on Energy Conversion*, vol. 37, no. 1, pp. 631-642, Aug. 2021.
[32] M. L. Thogersen, T. Sorensen, P. Nielsen *et al.*, "Introduction to wind turbine wake modelling and wake generated turbulence," Risø National Laborator, EMD Int. A/S, Aalborg, Denmark, 2006.
[33] Gurobi Optimization. (2024, Dec.). Gurobi software. [Online]. Available: https://www.gurobi.com/downloads/gurobi-software/
[34] *Short-circuit Current Calculation of Renewable Energy Power Generation Stations and Connection Systems – Part 1: Wind Power Generation*, GB/T 44659.1-2024, 2024.
[35] Iberdrola. (2024, Dec.). Saint-Brieuc: Iberdrola's first large-scale offshore wind power project in Brittany. [Online]. Available: https://www.iberdrola.com/about-us/what-we-do/offshore-wind-energy/saint-brieuc-offshorewind-farm
[36] UC Cable. (2024, Dec.). UC XLPE catalogue. [Online]. Available: http://www.ucable.com.my/images/products/UC%20XLPE%20Catalogue.pdf
[37] Goldwind. (2024, Dec.). Goldwind GWH171-6.25MW. [Online]. Available: https://www.goldwind.com/cn/windpower/product-gwh/
[38] R. Srikakulapu and U. Vinatha, "Combined approach based on ACO with MTSP for optimal internal electrical system design of large offshore wind farm," in *Proceedings of 2018 International Conference on Power, Instrumentation, Control and Computing*, Thrissur, India, Jan. 2018, pp. 1-6.
[39] R. D. Zimmerman, C. E. Murillo-Sánchez, and R. J. Thomas, "MATPOWER: steady-state operations, planning, and analysis tools for power systems research and education," *IEEE Transactions on Power Systems*, vol. 26, no. 1, pp. 12-19, Feb. 2011.
[40] Y. Huang, T. Ding, P. Wang *et al*., "Linearized AC power flow model based interval total transfer capability evaluation with uncertain renewable energy integration," *International Journal of Electrical Power & Energy Systems*, vol. 154, p. 109440, Dec. 2023.

Shuaifeng Wang received the B.S. degree from University of South China, Hengyang, China, in 2021. He is currently working toward the Ph.D. degree with the College of Electrical and Information Engineering, Hunan University, Changsha, China. His research interests include active distribution network and optimization of wind farm.

Sheng Huang received the M.S. and Ph.D. degrees from the College of Electrical and Information Engineering, Hunan University, Changsha, China, in 2012 and 2016, respectively. He is currently a Professor with the College of Electrical and Information Engineering, Hunan University. His research interests include renewable energy generation, modeling and integration of wind power, control of energy storage system, and voltage control.

Juan Wei received the B.S. and M.S. degrees in electrical engineering from North China Electric Power University, Beijing, China, in 2011 and 2014, respectively, and the Ph.D. degree from the College of Electrical and Information Engineering, Hunan University, Changsha, China, in 2022. She is currently an Assistant Professor with the College of Electrical and Information Engineering, Hunan University. Her research interests include wind power modeling and control, renewable energy generation, power system economic and secure operation, and motor control.

Qiuwei Wu obtained the Ph.D. degree in electrical engineering from Nanyang Technological University, Singapore, in 2009. His research interests include distributed optimal operation and control of low-carbon power and energy systems, in particular, distributed optimal control of wind power, distributed congestion management, voltage control and service restoration of active distribution network, optimal operation of integrated energy system, and data-driven and artificial intelligence (AI) empowered optimal operation.

Wenbo Tang received the master's degree from Hunan University, Changsha, China, in 2013. He is currently pursuing the Ph.D. degree in energy and power engineering at the same university. He is a Senior Engineer of Electric Power Engineering and a Level-two Technician for Substation Attendant. Currently, he serves as the Deputy Chief Engineer of the Disaster Prevention and Mitigation Engineering Institute, State Grid Hunan Electric Power Research Institute, Changsha, China. His research interests include adjustable shaft line test platform for wind turbine and construction of disaster warning platform.

Lu Zhou received the M.S. degree from Hunan University, Changsha, China, in 2010. She is the Deputy Director of the New Energy Center at Huadian Electric Power Research Institute and an Industry Mentor for graduate students at Huazhong University of Science and Technology, Wuhan, China. Her research interests include advanced wind power, renewable energy forecasting, and intelligent energy system.

Shoudao Huang received the B.E. and Ph.D. degrees in electrical engineering from Hunan University, Changsha, China, in 1982 and 2003, respectively. He is currently a Professor with the College of Electrical and Information Engineering, Hunan University. His research interests include motor drive, power electronics, and control system.